Lab on a Chip

PAPER

View Article Online
View Journal

Cite this: DOI: 10.1039/d0lc00660b

Multi-step processing of single cells using semi-permeable capsules†

Greta Leonaviciene, ‡[a] Karolis Leonavicius, ‡[a] Rolandas Meskys[b] and Linas Mazutis *[a]

Received 26th June 2020,
Accepted 23rd September 2020

DOI: 10.1039/d0lc00660b

rsc.li/loc

Droplet microfluidics technology provides a powerful approach to isolate and process millions of single cells simultaneously. Despite many exciting applications that have emerged based on this technology, workflows based on multi-step operations, including molecular biology and cell-based phenotypic screening assays, cannot be easily adapted to droplet format. Here, we present a microfluidics-based technique to isolate single cells, or biological samples, into semi-permeable hydrogel capsules and perform multi-step biological workflows on thousands to millions of individual cells simultaneously. The biochemical reactions are performed by changing the aqueous buffer surrounding the capsules, without needing sophisticated equipment. The semi-permeable nature of the capsules' shell retains large encapsulated biomolecules (such as genome) while allowing smaller molecules (such as proteins) to passively diffuse. In contrast to conventional hydrogel bead assays, the approach presented here improves bacterial cell retention during multi-step procedures as well as the efficiency of biochemical reactions. We showcase two examples of capsule use for single genome amplification of bacteria, and expansion of individual clones into isogenic microcolonies for later screening for biodegradable plastic production.

Introduction

Modern molecular biology research increasingly relies on high-throughput analytical methods to process complex samples at single-cell or single-molecule resolution.[1–3] Compartmentalization of individual cells, DNA, enzymes, or other biomolecules in water-in-oil droplets (or other forms of microscopic compartments) can assist this effort by enabling massively parallel analysis with a throughput orders of magnitude higher when compared to the microtiter plate platform.[4–6] However, many biological methods are built on sequential sample processing in order to initiate, modify, or terminate a reaction. These multi-step operations are difficult to implement in droplet, or other types of emulsion-based assays. Although some solutions, such as droplet fusion,[7,8] droplet reinjection,[9] splitting,[10] and sorting,[11,12] enables multi-step procedures,[13–16] however, the required expertise and complexity of fluidic operations often limits the broader use of such approaches. Sequential sample processing can become very challenging in microbiology assays when encapsulated bacteria, or their genetic material, has to be processed through a series of independent reactions.[17] For example, for the amplification and analysis of genetic material of microorganisms, it may be necessary to perform cell lysis, a step that might be inhibitory or incompatible with subsequent enzymatic step(s).

To circumvent some of the inherent limitations of microdroplet systems several hydrogel-bead based approaches have been proposed[18–20] with the key feature relying on cell embedding into a hydrogel mesh so that each biochemical reaction could be performed independently from the proceeding step. The hydrogel-bead systems have been successfully applied in a variety of biochemical reactions to perform phenotypic[21,22] or genotypic assays,[19,23,24] and screening.[20,25] However, most of the hydrogel-bead based methods reported to-date suffer from a few major drawbacks that limit the scope of biological applications. First, during hydrogel bead generation and gelation, a significant fraction of encapsulated cells is typically lost as cells tend to be adsorbed at the water–oil interface.[26] Second, the uniform permeability of the hydrogel mesh, although useful in some applications, precludes the selective retention and exchange of reagents between the encapsulated biomaterial and surrounding media, and may require further polymer grafting to retain cellular biomolecules.[24] Third, as encapsulated species become physically entrapped in the hydrogel matrix the compressive stress imparted by the polymer negatively

[a] Institute of Biotechnology, Life Science Centre, Vilnius University, 7 Sauletekio av., Vilnius, LT-10257, Lithuania. E-mail: linas.mazutis@bti.vu.lt
[b] Institute of Biochemistry, Life Science Centre, Vilnius University, 7 Sauletekio av., Vilnius, LT-10257, Lithuania

† Electronic supplementary information (ESI) available: ESI Fig. S1–S13, ESI Video S1, ESI Note. See DOI: 10.1039/d0lc00660b

‡ Contributed equally to this work.

impacts cell growth[27] and physiological response,[22,28] whilst the biochemical reaction efficiency and sensitivity can be affected by steric hindrance and reduced diffusivity[29–32] or undesirable electrostatic interactions with the hydrogel mesh.[26,33] Consequently, liquid droplets surrounded by a semi-permeable shell, could mitigate the aforementioned constraints and open a broader range of biological applications for isolation of individual cells to perform complex, multi-step biochemical reactions.

Herein, we combined advantages offered by droplet-based and hydrogel-based systems to create capsules containing a thin, semi-permeable shell. The shell acts as a passive sieve – retaining encapsulated, large molecular weight compounds while allowing smaller molecules (such as proteins) to diffuse through. Although various capsule synthesis approaches have been suggested previously,[34–42] no efforts have succeeded in making them compatible with multi-step molecular biology assays. We used an aqueous two-phase system (ATPS)[43] composed of dextran and acrylate-modified polyethylene glycol to generate the biocompatible hydrogel particles and showcased a few examples of sequential reactions on encapsulated species. Specifically, we compared genome amplification reaction efficiency on Gram-negative and Gram-positive bacterial cells and found that the DNA amplification yields tend to be higher in the capsule-based system. Capsules readily sustained multiple pipetting steps when performing complex biochemical reactions, and, in contrast to solid-hydrogel beads, retained a significantly larger fraction of encapsulated bacteria. We anticipate that the relatively simple generation of semi-permeable capsules presented here will facilitate the development of new single-cell assays in biology.

Results

Hydrogel capsule production

Concentric capsules (liquid droplets surrounded by the semi-permeable shell) can be used for many interesting biological applications as micro-reactors for the isolation of individual cells to perform complex biochemical reactions. Although previous efforts have been made to generate uniform capsules, yet poor control over shell integrity and concentricity has remained a significant challenge.[34,37,40,44] Because capsule's shell uniformity depends on the concentricity of ATPS droplets – a transient step in capsule synthesis process – we postulated that the density mismatch between the core and shell phases was driving the capsules' core off-centre before complete shell gelation could occur. To investigate this, we prepared dextran and polyethylene glycol diacrylate (PEGDA) solutions (see Materials and methods) and emulsified using a co-flow microfluidics device where each phase is introduced separately into a chip (Fig. 1a). Once encapsulated, dextran and PEGDA aqueous solutions mixed, yet the liquid–liquid phase separation quickly occurred during emulsion collection off-chip leading to the formation of monodisperse ATPS droplets. To solidify the shell of ATPS droplets *en masse*, we used photo-illumination[45] to induce fast (~2 min) PEGDA polymerization and form a hardened shell. As expected, and in agreement with previous studies,[34] during the capsule generation process, the dextran-rich core tended to migrate towards the outer interface, causing the particles to acquire complex topology and lose concentricity (Fig. S1†). As a result, a significant fraction of capsules contained uneven or ruptured shells that caused a premature release of the encapsulated material. Obviously, such defective capsules would hinder many biological applications that mandate efficient sample encapsulation, retention, and processing reproducibility. Importantly, reducing the density difference between the two aqueous phases, however, enabled a consistent generation of monodisperse and, most importantly, concentric ATPS droplets (Fig. 1b and S1†). We estimated that upon reaching the equilibrium, the core of concentric ATPS droplets comprised ~9.6% (w/v) dextran, and the shell comprised ~11% (w/v) PEGDA (Fig. S2†). To achieve the right balance between capsule uniformity, concentricity and mechanical

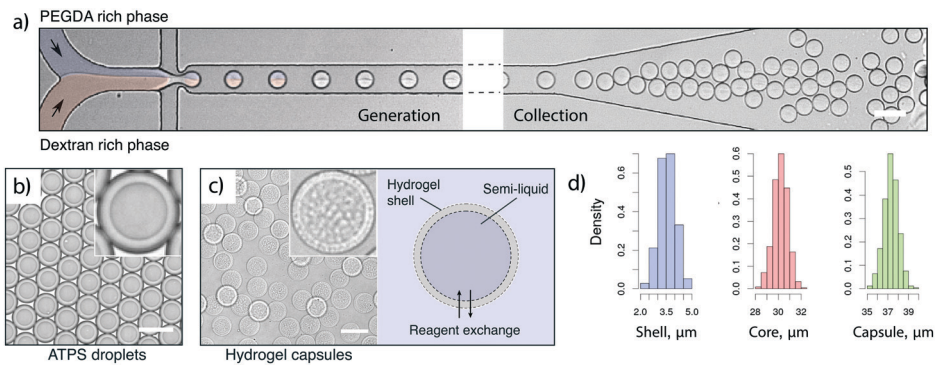

Fig. 1 Semi-permeable capsules successfully retain larger compounds and are uniform in size. (a) ATPS droplet generation using a co-flow microfluidics device. (b) Liquid–liquid phase separation in ATPS droplets resulting in dextran-rich core and PEGDA-rich shell. (c) Solidified hydrogel capsules and schematics. Capsules recovered from the emulsion and suspended in aqueous buffer, where PEGDA formed firm hydrogel shell and dextran phase formed the liquid-like core. (d) Histograms, derived from $N > 100$ measurements (compartments), indicate capsule shell thickness (3.56 ± 0.48 μm), capsule core (30.2 ± 0.6 μm) and overall diameter (37.3 ± 0.7 μm). Scale bars, 50 μm.

stability, we arrived at the composition containing blends of longer (MW 8K) and shorter (MW 575) PEGDA polymers, and aqueous dextran (MW 500K) solution (see Materials and methods). Whereas the longer PEGDA was required for efficient phase separation, the shorter PEGDA was added to increase shell stiffness and improve capsule mechanical stability by increasing the cross-linking density.[46] The resulting capsules contained a well-centered core enriched in dextran, and a solidified hydrogel-shell enriched in PEGDA (Fig. 1c). Note, the capsules' core became more viscous after the photo-polymerization (Fig. S2b†), which was presumably due to the presence of residual PEGDA, yet this seemed to have no negative effect on the biological assays exemplified in this work (see below).

Having established the method to produce concentric and uniform capsules, we then tested their stability at different physical and chemical conditions. Capsules remained highly uniform (with less than 2% size variation) after rigorous vortexing in aqueous buffer or washing in different organic solvents (Fig. S3†). Furthermore, capsules sustained multiple temperature cycles during PCR, as well as shear forces generated during flow cytometry (Fig. S4†). Using the microfluidic system reported here, the outer diameter of capsules could be tuned between 25 and 60 μm by simply changing the flow rates of the injected fluids. Larger ATPS droplets (≥80 μm), however, formed eccentric capsules with non-uniform shell thickness (Fig. S5†) and, thus, may require further optimizations of the composition of dextran/PEGDA blend. In the following sections, we showcase a few examples of semi-permeable 37 μm size capsule utility in multi-step procedures for genotypic and phenotypic analysis of individual bacterial cells.

Single-genome amplification following bacteria lysis

Nucleic acid analysis of individual bacterial cells in water-in-oil emulsions can be hindered by the preceding cell lysis step, leading to inefficient or non-uniform DNA amplification or, in case of hydrogel beads, significant cell loss during gel solidification. Bacterial lysis steps can be particularly problematic for single-step isothermal nucleic acid amplification methods (*e.g.*, multiple displacement amplification [MDA]) or working with Gram-positive bacteria, which are known to be much more resistant to thermolysis.[47]

To evaluate the semi-permeable capsule applicability in microbiology, we first compared the efficiency of MDA reaction on individual *Escherichia coli* bacterial cells in three different formats; 1) water-in-oil droplets, 2) hydrogel beads and 3) semi-permeable capsules (Fig. 2). For each test, a suspension of *E. coli* cells was encapsulated in a 20 picoliter (pl) volume droplets together with reagents required for lysis/MDA reaction, hydrogel bead, or capsule generation (see Materials and methods for further details). After encapsulation, the observed occupancy by *E. coli* cells in each assay followed Poisson distribution with a mean lambda value ~0.2, which indicated no significant encapsulation bias

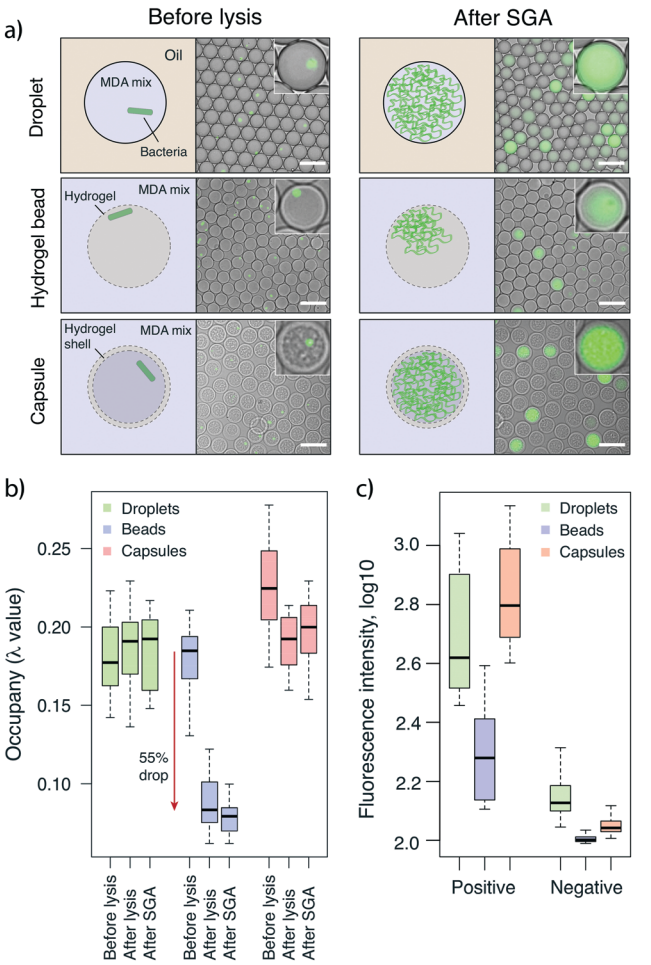

Fig. 2 Single genome amplification on individual *E. coli* cells was more efficient in semi-permeable capsules than either hydrogel beads or droplets. (a) Schematics depicting each assay with corresponding digital images showing fluorescence intensity of each assay before cell lysis and after single-genome amplification (SGA) reaction (see Material and methods for further details). Exposure times used for fluorescent microscopy were, before lysis – 1 s, after SGA – 10 ms. (b) Lambda value (occupancy) measurements after *E. coli* encapsulation, lysis, and SGA reaction in three assay formats. Water-in-oil emulsion (green), hydrogel beads (blue), and semi-permeable capsules (red). Boxplots are derived by measuring the fluorescence of >400 compartments from each sample. Note the significant drop in lambda value after the lysis step using hydrogel beads. (c) Boxplots representing mean fluorescence intensity in positive and negative (empty) post-SGA compartments. Boxplots were derived by measuring the fluorescence of 558 droplets, 511 hydrogel beads, and 491 capsules. Scale bars, 50 μm.

between assays. However, significant differences emerged after the cell lysis step. Whereas the number of positive compartments in water-in-oil droplets remained similar (Fig. 2b, green), the hydrogel-beads lost ~55% of the cells (Fig. 2b, blue). In capsules, the cell loss was insignificant, at approximately ~15% (Fig. 2b, red). Closer microscopy analysis revealed that such a notable drop in occupancy could be attributed to the bacteria's tendency to localize at the proximity of the hydrogel/oil interface (Fig. 2a and S6†).

In support of this notion, previous reports have shown that encapsulated bacteria tend to distribute at the surfaces[48]

and water/oil interface.[26,49,50] As a result of this distribution, gDNA released during the lysis step becomes susceptible to diffusion out of the hydrogel mesh and eventual loss. In capsules, however, the presence of hydrogel-shell prevented the majority of cells from reaching the outer (oil) phase, thereby improving the retention of cell lysate. Noteworthy, the cell partition properties can be tuned by adjusting the ionic species, electrostatic potential, or molecular properties of dextran/PEGDA phases.[51–53]

Fluorescence measurements of post-MDA compartments revealed that single-genome amplification (SGA) reaction on individual cells was more efficient in capsules as compared with hydrogel-beads or droplets (Fig. 2). The increased SGA reaction yield in capsules could be attributed to the liquid-like core, which does not interfere with the synthesis of long DNA molecules (>10 kb) generated by phi29 DNA polymerase. In hydrogel beads, however, the newly synthesized DNA is embedded in the hydrogel mesh and physically confined, thereby causing less efficient enzymatic replication. In support of this notion, the SGA reaction yield in water-in-oil droplets (liquid state) was ~2 times higher than in beads (hydrogel state), as shown in Fig. 2c (green and blue boxplots). Comparing the DNA synthesis efficiency in capsules *vs.* water-in-oil droplets (Fig. 2, red and green boxplots), we observed mild reaction improvement in capsules, which we attributed to the exchange of reaction components through a semi-permeable membrane. In other words, the amount of SGA reagents (such as dNTPs, oligonucleotides, DNA polymerase), in the capsule-based assay was not defined by the droplet volume[9] but could be continuously replenished through a semi-permeable membrane. Alternatively, these results could also be explained by more efficient bacteria lysis: the capsules were suspended in lysis buffer containing lysozyme and proteinase K enzymes prior to DNA amplification, while in micro-droplet assay, the use of protease is prohibitive because of incompatibility with SGA. Repeating the same type of experiment on *Bacillus subtilis* bacteria also generated higher fluorescence signal in capsules, confirming the reproducibility of the SGA reaction improvement across different bacteria species (Fig. S7†). Moreover, the capsule-based SGA reaction showed higher amplification uniformity and better signal-to-noise ratio.

We anticipated that the differences in single-genome amplification efficiency should become even more pronounced on Gram-positive microorganisms whose lysis requires harsher conditions that are either inhibitory or detrimental to subsequent enzymatic steps. To verify this, we separately encapsulated *Rhodococcus rhodochrous* and *Streptococcus mutans* bacteria and subsequently lysed them at different conditions (Table 1). Following cell lysis, the capsules were washed in neutral buffer and transferred directly to the MDA reaction mix to initiate DNA synthesis. Out of six conditions tested, the two-step lysis approach involving lysozyme-induced lysis at 37 °C for 30 min followed by proteinase K and SDS treatment at 50 °C for 30 min

Table 1 Bacteria lysis conditions and single genome amplification reaction efficiency

SGA reaction condition	Bacteria lysis	First step	Second step	Reaction efficiency
Ref.	One-step lysis in droplets	50 U μL^{-1} lysozyme, 0.1% (v/v) Triton X-100, 1 mM DTT, 1× MDA reaction mix incubated for 12 h at 30 °C	None	25% (strep.) 8% (rhod.)
1	One-step lysis in capsules	50 U μL^{-1} lysozyme, 0.1% (v/v) Triton X-100, 1 mM DTT, 1× MDA reaction mix incubated for 12 h at 30 °C	None	25% (strep.) 4% (rhod.)
2	Two-step lysis in capsules	50 U μL^{-1} lysozyme, 0.1% (v/v) Triton X-100, 1 mM EDTA, 10 mM Tris–HCl [pH 7.5]. Incubation for 30 min at 37 °C	Capsules washed and dispersed in MDA mix for 12 h at 30 °C	26% (strep.) 3% (rhod.)
3	Two-step lysis in capsules	50 U μL^{-1} lysozyme, 0.1% (v/v) Triton X-100, 1 mM EDTA, 200 $\mu g\ ml^{-1}$ proteinase K. 10 mM Tris–HCl [pH 7.5]. Incubation at 37 °C for 30 min followed by 50 °C for 30 min	Capsules washed and dispersed in MDA mix for 12 h at 30 °C	20% (strep.) 58% (rhod.)
4	Two-step lysis in capsules	50 U μL^{-1} lysozyme, 0.1% (v/v) Triton X-100, 1 mM EDTA., 10 mM Tris–HCl [pH 7.5]. Incubation for 30 min at 37 °C	Add 200 $\mu g\ ml^{-1}$ proteinase K and incubate at 50 °C for 30 min. Washed and dispersed in MDA mix for 12 h at 30 °C	15% (strep.) 57% (rhod.)
5	Two-step lysis in capsules	0.5 M NaOH and 1% (w/v) SDS. Lysis at room temperature for 5 min	Neutralized, washed and dispersed in MDA mix for 12 h at 30 °C	33% (strep.) 48% (rhod.)
6	Two-step lysis in capsules	50 U μL^{-1} lysozyme solution, 0.1% (v/v) Triton X-100, 1 mM EDTA, 10 mM Tris–HCl [pH 7.5]. Lysis at 37 °C for 30 min	Add 200 $\mu g\ ml^{-1}$ proteinase K and 1% (w/v) SDS and incubated at 50 °C for 30 min. Washed and dispersed in MDA mix for 12 h at 30 °C	84% (strep.) 99% (rhod.)

generated the highest numbers of positive reactions (condition #6 in Table 1 and Fig. S8†). Thus, combining results obtained with Gram-negative and Gram-positive bacteria, we conclude that capsules not only efficiently retain the cells and their genetic material released upon lysis but more importantly, can be processed through a series of incompatible reactions and generate increased yields of amplified DNA.

If the capsule's shell provides an efficient physical barrier for retaining large molecular weight biomolecules, such as a bacterial chromosome or amplified gDNA, then what are the smallest DNA fragments that capsules can still retain? We sought to answer this question by generating 320, 567, and 1050 bp DNA fragments by PCR and following their diffusion between the compartments. As illustrated in Fig. 3, the capsules efficiently retained DNA fragments larger than 567 bp, the molecular weight of which approximately corresponds to 340 kDa. Smaller DNA fragments (320 bp size) diffused between the capsules as witnessed by the appearance of low fluorescence compartments and increased post-PCR occupancy value (see ESI† Note and Fig. S9). Using the Kratky–Porod equation[54] we estimated that PCR fragments (320, 567, and 1050 bp) have radii of gyration on the order of 26, 40 and 60 nm. Considering these values and diffusivity results, it can be approximated that the average pore size of the hydrogel shell is approximately ~30 nm. Scanning electron microscopy analysis revealed an average pore size 55 ± 31 nm (Fig. S10†). Finally, to confirm that the expected size DNA fragments were indeed generated during PCR, we dissolved the capsules in alkaline solution, extracted the DNA, and performed electrophoresis. As expected, PCR was highly specific and produced the amplicons of the expected size (Fig. S11†).

Combined cell culture and phenotypic analysis

In addition to nucleic acid amplification and analysis, many microbiology assays also rely on phenotypic cell characterization. This commonly requires bacterial culture, induced gene expression, and subsequent analysis of proteins or metabolites that serve as a phenotypic readout. We demonstrated the use of capsules for cell culture and screening for metabolic activity in isogenic micro-colonies originating from a single bacterium.

We first evaluated whether the capsules could be used as micro-chemostats for cell culture applications. For that purpose, using the same microfluidics device as indicated in Fig. 1, we encapsulated *E. coli* and then immersed capsules in the growth medium for 4 hours at 37 °C. Following SGA results, we postulated that passive diffusion of growth media through the semi-permeable capsule shell would ensure fast cell growth until the entire capsule core is filled with bacteria mass. In the droplet case, however, the critical cell mass should be limited by the available nutrients inside the single compartment where a bacteria clone resides. To test this, we used time-lapse microscopy to continuously monitor individual cells, their growth, and expansion into micro-colonies (ESI† Video S1). Combining this digital data with fluorescence analysis, we estimated that in the capsules, a single bacterial cell expanded into a colony containing, on average, 90 cells within approximately 4 hours (Fig. 4). In comparison, water-in-oil droplets generated smaller micro-colonies, containing 30 cells on average (Fig. 4). As an additional advantage, the analysis based on fluorescence signal was considerably easier in capsules, because the background from auto-fluorescent LB media could be removed in a few washing steps, leading to an increased signal-to-noise ratio (Fig. S12†).

Having shown the cell growth and isogenic colony formation, we then applied capsules for phenotypic analysis of bacteria producing polyhydroxybutyrate (PHB) – an environmentally important biodegradable plastic.[55,56] Identifying the metabolic products of microorganisms can be a challenge because it requires simultaneous phenotypic (PHB synthesis) and genotypic (nucleic acid quantification) readouts. To demonstrate that such analysis is possible with semi-permeable capsules, we used *E. coli* (DH5α) strain transformed with the pBHR68 vector, harboring genes (phaC, phaA and phaB) for PHB synthesis.[57] We

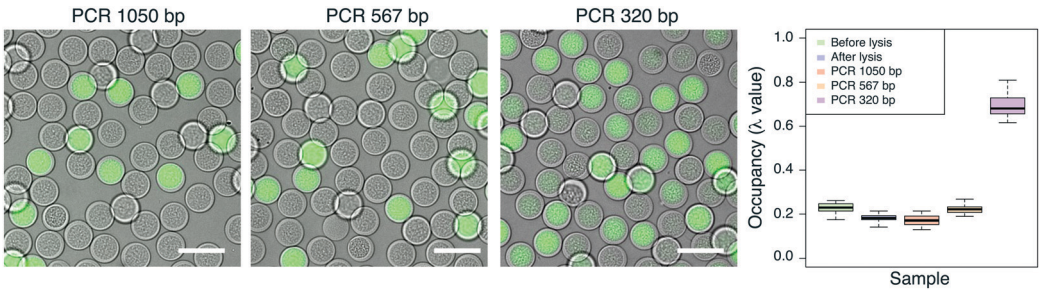

Fig. 3 Capsules retain DNA fragments larger than 500 bp (340 kDa). On the left, merged images showing the capsules after the synthesis of different length PCR amplicons: ompA (1050 bp), kdsC (567 bp), 16S rRNA (320 bp). On the right, boxplots, representing lambda value (the mean number of bacteria in each capsule following Poisson distribution) before and after cell lysis, and after PCR with corresponding PCR amplicons. Histograms are derived from samples by measuring fluorescence of $N > 800$ positive capsules for each sample. Scale bars, 50 μm.

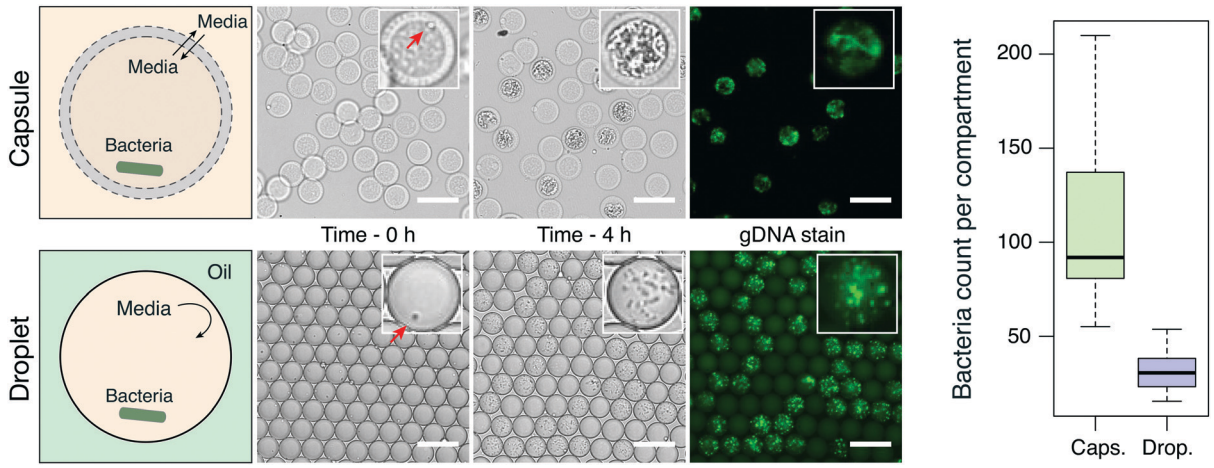

Fig. 4 Expansion of *E. coli* in capsules resulted in more cells than in droplets. Left: schematics depicting capsule-based and droplet-based assay. In capsules, the growth media ingredients can diffuse through porous hydrogel shell, while in droplet-based approach, the amount of the ingredients is limited by droplet volume. Digital images show bacteria growth in capsules (top row) and in droplets (bottom row) at 0 and 4 hours of cell culture at 37 °C. The red arrows indicate a single bacterium at time 0. Fluorescent images were obtained after staining with SYBR Green I dye. Right: boxplots, representing bacteria counts after 4 hours of incubation in capsules (caps.) and in droplets (drop). Boxplots were derived by measuring 20 droplets and 30 capsules. Scale bars, 50 μm.

loaded cells in microfluidic capsules, cultivated them into micro-colonies for 6 hours and then induced PHB synthesis by adding isopropyl β-D-1-thiogalactopyranoside (IPTG). After 8 hours of induction, we verified PHB formation in live cells using Nile red dye, which stains PHB granules[58] (Fig. 5 and S13†). However, Nile red binds to cell membranes because of its lipophilicity, yielding a highly fluorescent signal in both positive and negative control samples. To circumvent the background fluorescence resulting from non-specific staining, we dissolved cell membranes with lysis reagents (condition #3 in Table 1), which increased the analytical sensitivity of positive-to-negative clones by approximately 10-fold (Fig. S13†). Finally, we used Nile red dye for PHB granules and SYBR Green I for gDNA, which allowed us to normalize PHB synthesis levels to bacteria count (Fig. 5). This type of normalization is critical for screening efficient producers rather than the fastest growing clones.

Discussion

Treatment and analysis of biological samples is based on sequential operations where new reagents are added, or removed, at a defined step during the reaction. Using droplet

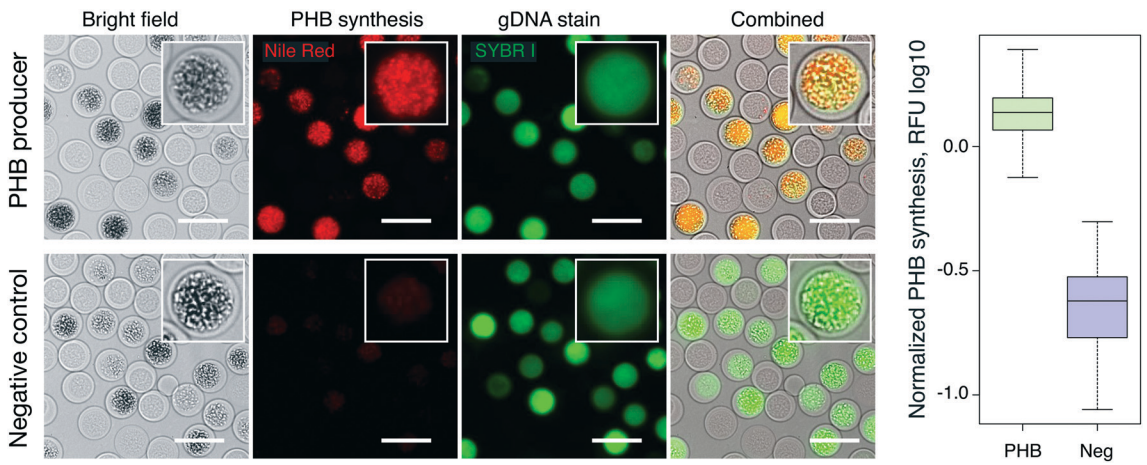

Fig. 5 Individual bacteria clones remain physiologically active and can be expanded into isogenic colonies inside the capsules. Left: capsules containing micro-colonies of positive (DH5α-pBHR68) and negative (DH5α-pTZ18R) clones. Bright-field images show colony size, Nile red staining shows PHB metabolite amount, SYBR I indicates bacteria quantity in individual capsules based on gDNA staining, and combined images show superimposed Nile red and SYBR I images. All staining was performed after cell lysis. Scale bars, 50 μm. Right: normalized PHB synthesis levels of positive (green) and negative (blue) clones. The ratio of Nile red to SYBR Green I was used for normalizing the PHB levels to bacteria count. Boxplots are derived from 107 and 78 measurements of positive and negative producer colonies, respectively. Scale bars, 50 μm.

microfluidics for these operations often requires complex technological solutions and specific skillset that is not readily available in many molecular biology laboratories. To bridge this gap, we report a simple and versatile approach to isolate individual cells or other biological samples in semi-permeable capsules and to conduct multi-step sequential biochemical reactions by simply changing the aqueous solution in which capsules are dispersed. The semi-permeable nature of the capsules' shell ensures that it retains large entities (>340 kDa) inside, while smaller molecules (such as proteins and reagents) can passively move between the interior and exterior environments. As such, the capsules are well suited for conducting multi-step, massively parallel reactions on hundreds of thousands of encapsulated cell and molecular species using a single laboratory tube. In contrast to conventional hydrogel-bead based systems, the capsules retain a much larger fraction of encapsulated cells and ensure better yields of the single-genome amplification reaction. Capsules do not disintegrate when using harsh chemicals (*e.g.*, lysis reagents) and remain physically intact during pipetting, flow cytometry, or other laboratory procedures, and thus are well-suited for conducting different single-cell assays. To demonstrate the capsule use in biology, we performed sequential and incompatible reactions on single Gram-positive and Gram-negative bacterial cells, and obtained increased yields of individually amplified genomes, presumably due to efficient reagent exchange through the semi-permeable shell. As yet another example, we showed that individual bacteria cells maintain their physiological activity inside the capsules and can be quickly expanded to isogenic microcolonies. Using a fluorescence-based readout, we showed the feasibility of phenotype-based screening of bacteria clones producing polyhydroxybutyrate polymer. Thus, encapsulated cells can be harvested and interrogated to characterize their biological activity and phenotypic features.

However, the capsule-based approach reported here is not without some limitations. The capsules do not retain small molecules, such as enzymes making screening of secreted proteins or metabolites problematic. Although, it should be possible to tune the pore size of hydrogel shell by changing the relative concentration and molecular weight of PEGDA, or use of the porogen (PEG), yet finding the right polymer blend composition while maintaining capsule concentricity will require further efforts in the future. Using the reported dextran/PEGDA polymer blend, the capsule's diameter is limited to the 25–60 μm range – beyond which the generation of larger size concentric capsules becomes increasingly difficult to achieve. Despite these few constraints, we expect the benefits will greatly outweigh the few limitations and that the capsule-based approach reported here will find useful applications in biology and biotechnology for screening, analysis, and sequencing of individual cells. The platform itself is simple and inexpensive to implement, requiring two syringe pumps and a microscope, and should find broad utility. Finally, considering the biocompatibility, semi-permeability, and mechanical stability of capsules, one can easily envision other applications that could benefit from this technology. For example, performing capsule-based phenotypic screening using conventional FACS instrument followed by DNA (or RNA) sequencing of the sorted cells would be feasible using these capsules.

Materials and methods

Device fabrication and operation

The polydimethylsiloxane (PDMS) microfluidic device was fabricated and operated using standardized protocol as described.[12]

Preparation of ATPS

All chemicals were ordered from Sigma-Aldrich and Fisher Scientific. ATPS droplets were prepared using 5.5% (w/v) dextran (MW 500K), 3% (w/v) PEGDA (MW 8K), 3% (v/v) PEGDA (MW 575), 0.1% (w/v) LAP (lithium phenyl-2,4,6-trimethylbenzoylphosphinate), 1× DPBS (Gibco, 14190144). Other concentrations of PEGDA (MW 8K) and PEGDA (MW 575) could be used following Table 2. In all compositions tested, the concentration of dextran (MW 500K) and LAP were constant. The solutions containing all ingredients were mixed and centrifuged in a table centrifuge at maximum speed for 30 minutes to induce liquid–liquid phase separation. The bottom (dextran-rich) phase was used to re-suspend bacterial cells. Noteworthy, if the turbidity and phase separation are not observed, we would recommend supplementing the prepared PEGDA/dextran mix with a low amount of longer PEGDA until turbidity and subsequent phase separation are obtained. We noticed that even poorly calibrated laboratory pipets could cause inefficient formation of biphasic system.

Preparation of hydrogel beads

The mixture of 6% (v/v) PEGDA (MW 575) and 0.1% (w/v) LAP in 1× DPBS was used for hydrogel bead preparation and bacteria embedding following emulsification and cross-linking conditions described below.

Table 2 The composition of capsule's shell and applications tested

	Composition	Applications
1.	3% (w/v) PEGDA (MW 8K) + 3% (v/v) PEGDA (MW 575)	Culture, MDA, PCR (≥567 bp)
2.	2.5% (w/v) PEGDA (MW 8K) + 4% (v/v) PEGDA (MW 575)	Culture, MDA, PCR (≥567 bp)
3.	2.1% (w/v) PEGDA (MW 8K) + 5% (v/v) PEGDA (MW 575)	PCR (≥567 bp)

Preparation of microbial cells

Escherichia coli (MG1655 and DH5α), *Bacillus subtilis* (SHgw), *Rhodococcus rhodochrous* PY11 (DSM 101666)[59] as well as pBHR68[57] and pTZ18R plasmids were from the laboratory collection. *Streptococcus mutans* (UA159) was provided by Prof. Edita Sužiedėlienė (Vilnius University, Institute of Biosciences, Lithuania). DH5α strain was transformed with pBHR68 plasmid, harboring three genes (phaC, phaA and phaB) from PHB synthesis pathway. As a negative control, DH5α transformed with pTZ18R vector was used. Prior the encapsulation bacteria were suspended in dextran-rich phase. Working with DH5α strain, dextran-rich phase was supplemented with 100 μg ml^{-1} ampicillin.

Emulsification

Droplets, hydrogel beads and capsules were generated using microfluidics chip 20 μm height and having a nozzle 15 μm wide (Fig. 1). Typical flow-rates used were: PEGDA-rich phase – 50 μl h^{-1}, dextran-rich phase or 1× DPBS (with/without bacteria) – 50 μl h^{-1} and droplet stabilization oil (Droplet Genomics, DG-DSO-20) – 500 μl h^{-1}. Due to the increased viscosity of biphasic system, droplet breakup by jetting mechanism could be observed, which could shift to dripping mode by adjusting the flow rates of a system.

Cross-linking

Emulsions were collected in a 1.5 ml tube and immediately cross-linked by exposure under 365 nm wavelength using high-intensity UV inspection lamp, UVP (UVP, 95-0127-01) for 2.5 minutes. ATPS droplets for bacteria culture experiments were exposed to 405 nm laser (Besram Technology Inc. module TEM00) at 1 W cm^{-2} for 20 seconds. After hardening the PEGDA shell resulting capsules were recovered from the emulsion using commercial emulsion breaker (Droplet Genomics, DG-EB-1).

Lysis and DNA amplification in hydrogel beads and capsules

Lysis of encapsulated bacteria was performed by suspending hydrogel beads or capsules in lysis buffer containing: 50 U μl^{-1} Ready-Lyse lysozyme solution (Lucigen, R1804M), 200 μg ml^{-1} proteinase K (Invitrogen, AM2546), 0.1% (v/v) Triton X-100 (Sigma-Aldrich, T8787-100ML), 1 mM EDTA (Invitrogen, 15575020), 10 mM Tris–HCl [pH 7.5] (Invitrogen, 15567027). Hydrogel beads and capsules suspended in lysis buffer were incubated for 30 min at 37 °C followed by additional 30 min incubation at 50 °C. After lysis, hydrogel beads and capsules were washed three times in a washing buffer (10 mM Tris–HCl [pH 7.5] and 0.05% (v/v) Triton X-100). For lysis conditions on gram-positive (*Rhodococcus rhodochrous* and *Streptococcus mutans*) bacteria refer to Table 1. MDA reaction was then performed by suspending capsules and hydrogel beads in MDA reaction buffer containing 0.5 U μl^{-1} phi29 DNA polymerase (Thermo Scientific, EP0092) and 0.002 U μl^{-1} pyrophosphatase (Thermo Scientific, EF0221) following manufacturer's recommendations. Bulk-like PCR was used to amplify specific regions of 16S rRNA, kdsC and ompA genes corresponding to 320, 567 and 1050 bp fragments, respectively. Each amplification was performed for 35 cycles with KAPA PCR kit (KAPABiosystems, KK2602) according to manufacturer's recommendations. In all enzymatic reactions, the close-packaged capsules and hydrogel beads occupied approximately 40–50% of the final reaction volume.

Lysis and DNA amplification in droplets

To perform *E. coli*, *B. subtilis*, *R. rhodochrous* and *S. mutans* lysis in droplets, bacteria were re-suspended in 10 mM Tris–HCl [pH 7.5] and co-encapsulated with Ready-Lyse lysozyme solution, Triton X-100, phi29 DNA polymerase buffer and DTT at the final concentration of 50 U μl^{-1}, 0.1% (v/v), 1× and 1 mM, respectively. When cell lysis and MDA reaction was performed simultaneously, the final reaction composition was: 1× reaction buffer for phi29 DNA polymerase, 25 μM Exo-resistant random primer (Thermo Scientific, SO181), 1 mM dNTP Mix (Thermo Scientific, R0192), 1 mM DTT (Thermo Scientific, 707265ML), 0.1% (v/v) Triton X-100 (Sigma-Aldrich, T8787-100ML), 50 U μl^{-1} Ready-Lyse™ lysozyme solution (Lucigen, R1804M), 0.5 U μl^{-1} phi29 DNA polymerase (Thermo Scientific, EP0092) and 0.002 U μl^{-1} pyrophosphatase (Thermo Scientific, EF0221). The encapsulation conditions as well as MDA reaction conditions were the same as with capsules.

Imaging of processed bacteria

Droplets, hydrogel beads and capsules before and after lysis, and after nucleic acid amplification were stained with 1× SYBR Green I dye (Invitrogen, S7563) and analyzed under inverted fluorescence microscope using the following settings: magnification – 10×, filter – FITC, gain – 1, 20% intensity of blue light source used for excitation and exposure time were varied depending on the analysis step. Images were recorded using digital camera (Nikon eclipse Ti at 12 bit resolution).

Capsule analysis by flow cytometry

The post-SGA capsules were stained with 1× SYBR Green I dye (Invitrogen, S7563) and analyzed on sapphire microfluidics platform (Droplet Genomics, DG-SPH-1). A total of 150 000 capsules were measured using a 488 nm diode laser (1 mW) focused to a 40 μm channel.

Scanning electron microscopy

SEM was performed on a Helios Nanolab 650 (FEI) instrument. Capsules were deposited on a silicon wafer pre-treated with an oxygen plasma, air-dried and imaged at a 100 000× magnification using 2.0 kV and 25 pA parameters.

Capsule solubilization and DNA extraction

Capsules were dissolved in the presence of 1 M NaOH at 50 °C for 10 minutes and then neutralized by adding equimolar amount of 1 M acetic acid. PCR and WGA products from dissolved capsules were extracted and concentrated using 1.8× Agencourt AMPure XP magnetic beads (Beckman Coulter, A63881) and analyzed on 1% agarose gel.

Bacteria cultivation inside capsules

All bacteria growth experiments were performed in disposable 30 × 15 mm Petri dishes. *E. coli* MG1655 bacteria encapsulated in capsules or droplets were cultivated in LB medium at 37 °C for 4–16 h, while the media for transformed DH5α strain was supplemented with 100 μg mL^{-1} ampicillin. After reaching exponential growth (4–6 h), polyhydroxybutyrate synthesis in DH5α was induced by adding 1 mM isopropyl β-D-1-thiogalactopyranoside (Thermo Scientific, R1171) followed by incubation at 30 °C for 8 h.

Imaging of encapsulated bacteria

Capsules and droplets with MG1655 cells were stained with 1× SYBR Green I (Invitrogen, S7563) dye and analyzed under inverted fluorescence microscope. DH5α strain was stained for 10 minutes with 0.5 μg ml^{-1} Nile red (Invitrogen, N1142) and analyzed using the following settings: magnification – 10×, filter – TXRED, gain – 1, exposure time – 100 ms, 40% intensity of green light source for excitation. The second round of imaging was performed after lysis (without the additional staining with Nile red) using the same conditions to evaluate the changes of fluorescence. For dual DH5α imaging, capsules were stained repeatedly with Nile red and SYBR Green I dyes. Images were taken using following settings: magnification – 10×, filters – FITC and TXRED, gain – 1, exposure time – 10 ms for FITC filter and 40 ms for TXRED, 20% and 40% intensity of blue and green light source for excitation, respectively. Images were recorded using Nikon eclipse Ti camera at 12 bit resolution on an inverted fluorescence microscope.

Data processing

Fluorescence data was obtained by manually outlining droplets, capsules and beads from brightfield images and then using these masks to segment fluorescence images. Data was managed and analyzed using R (v.3.5.3) and R studio (v.1.1.463). Capsule fluorescence was normalized to image background and image acquisition settings were kept the same during comparative experiments. Fluorescence was reported as logarithmic values to control the dynamic range, normalize dispersion and allow comparing dim and bright objects. Positive/negative capsule identification was achieved based on fluorescence data histogram analysis.

Author contributions

GS and KL performed experiments, RM provided guidance in microbiology experiments, LM supervised the study. GS, KL and LM analyzed the data and wrote the manuscript.

Conflicts of interest

The results of this work have been filed for a provisional patent application.

Acknowledgements

This work was supported by the European Social Fund according to the activity "Improvement of researchers' qualification by implementing world-class R&D projects" of Measure [grant number 09.3.3-LMT-K-712-01-0056]. K. L. was partly supported by a Research Council of Lithuania postdoctoral award [grant number 09.3.3-LMT-K-712-02-0067] and partly by Droplet Genomics (Vilnius, Lithuania). We would also like to express our gratitude to Rūta Stanislauskienė, Vida Časaitė, Edita Sužiedėlienė and Jūratė Skerniškytė for providing valuable insights, advices and bacterial strains. We would like to thank Valdemeras Milkus and Emilis Gegevičius (Vilnius University, Lithuania) and Jonas Gasparavičius (Droplet Genomics, Lithuania) for supplying microfluidic devices used in this work.

References

1 K. Leonavicius, J. Nainys, D. Kuciauskas and L. Mazutis, Multi-omics at single-cell resolution: comparison of experimental and data fusion approaches, *Curr. Opin. Biotechnol.*, 2019, **55**, 159–166.
2 T. Stuart and R. Satija, Integrative single-cell analysis, *Nat. Rev. Genet.*, 2019, **20**, 257–272.
3 M. H. Spitzer and G. P. Nolan, Mass Cytometry: Single Cells, Many Features, *Cell*, 2016, **165**, 780–791.
4 M. T. Guo, A. Rotem, J. A. Heyman and D. A. Weitz, Droplet microfluidics for high-throughput biological assays, *Lab Chip*, 2012, **12**, 2146–2155.
5 A. M. Klein, *et al.*, Droplet barcoding for single-cell transcriptomics applied to embryonic stem cells, *Cell*, 2015, **161**, 1187–1201.
6 E. Z. Macosko, *et al.*, Highly Parallel Genome-wide Expression Profiling of Individual Cells Using Nanoliter Droplets, *Cell*, 2015, **161**, 1202–1214.
7 L. Mazutis, J. C. Baret and A. D. Griffiths, A fast and efficient microfluidic system for highly selective one-to-one droplet fusion, *Lab Chip*, 2009, **9**, 2665–2672.
8 D. J. Eastburn, A. Sciambi and A. R. Abate, Picoinjection enables digital detection of RNA with droplet rt-PCR, *PLoS One*, 2013, **8**, e62961.
9 L. Mazutis, *et al.*, Droplet-based microfluidic systems for high-throughput single DNA molecule isothermal amplification and analysis, *Anal. Chem.*, 2009, **81**, 4813–4821.

10 A. R. Abate and D. A. Weitz, Faster multiple emulsification with drop splitting, *Lab Chip*, 2011, **11**, 1911–1915.
11 J. C. Baret, *et al.*, Fluorescence-activated droplet sorting (FADS): efficient microfluidic cell sorting based on enzymatic activity, *Lab Chip*, 2009, **9**, 1850–1858.
12 L. Mazutis, *et al.*, Single-cell analysis and sorting using droplet-based microfluidics, *Nat. Protoc.*, 2013, **8**, 870–891.
13 L. Mazutis, *et al.*, Multi-step microfluidic droplet processing: kinetic analysis of an in vitro translated enzyme, *Lab Chip*, 2009, **9**, 2902–2908.
14 B. El Debs, R. Utharala, I. V. Balyasnikova, A. D. Griffiths and C. A. Merten, Functional single-cell hybridoma screening using droplet-based microfluidics, *Proc. Natl. Acad. Sci. U. S. A.*, 2012, **109**, 11570–11575.
15 B. Kintses, *et al.*, Picoliter cell lysate assays in microfluidic droplet compartments for directed enzyme evolution, *Chem. Biol.*, 2012, **19**, 1001–1009.
16 F. Lan, J. R. Haliburton, A. Yuan and A. R. Abate, Droplet barcoding for massively parallel single-molecule deep sequencing, *Nat. Commun.*, 2016, **7**, 11784.
17 F. Lan, B. Demaree, N. Ahmed and A. R. Abate, Single-cell genome sequencing at ultra-high-throughput with microfluidic droplet barcoding, *Nat. Biotechnol.*, 2017, **35**, 640–646.
18 Y. K. Jo and D. Lee, Biopolymer Microparticles Prepared by Microfluidics for Biomedical Applications, *Small*, 2020, **16**, 1903736.
19 Z. Zhu, *et al.*, Highly sensitive and quantitative detection of rare pathogens through agarose droplet microfluidic emulsion PCR at the single-cell level, *Lab Chip*, 2012, **12**, 3907–3913.
20 S. J. Spencer, *et al.*, Massively parallel sequencing of single cells by epicPCR links functional genes with phylogenetic markers, *ISME J.*, 2016, **10**, 427–436.
21 Y. Ma, M. P. Neubauer, J. Thiele, A. Fery and W. T. S. Huck, Artificial microniches for probing mesenchymal stem cell fate in 3D, *Biomater. Sci.*, 2014, **2**, 1661–1671.
22 M. Li, *et al.* A Gelatin Microdroplet Platform for High-Throughput Sorting of Hyperproducing Single-Cell-Derived Microalgal Clones, *Small*, 2018, **14**, 1803315.
23 H. F. Zhang, G. Jenkins, Y. Zou, Z. Zhu and C. J. Yang, Massively Parallel Single-Molecule and Single-Cell Emulsion Reverse Transcription Polymerase Chain Reaction Using Agarose Droplet Microfluidics, *Anal. Chem.*, 2012, **84**, 3599–3606.
24 A. Rakszewska, R. J. Stolper, A. B. Kolasa, A. Piruska and W. T. Huck, Quantitative Single-Cell mRNA Analysis in Hydrogel Beads, *Angew. Chem., Int. Ed.*, 2016, **55**, 6698–6701.
25 T. Kamperman, M. Karperien, S. Le Gac and J. Leijten, Single-Cell Microgels: Technology, Challenges, and Applications, *Trends Biotechnol.*, 2018, **36**, 850–865.
26 M. Walser, *et al.*, Novel method for high-throughput colony PCR screening in nanoliter-reactors, *Nucleic Acids Res.*, 2009, **37**, e57.
27 K. Alessandri, *et al.*, Cellular capsules as a tool for multicellular spheroid production and for investigating the mechanics of tumor progression in vitro, *Proc. Natl. Acad. Sci. U. S. A.*, 2013, **110**, 14843–14848.
28 H. H. Tuson, *et al.*, Measuring the stiffness of bacterial cells from growth rates in hydrogels of tunable elasticity, *Mol. Microbiol.*, 2012, **84**, 874–891.
29 D. C. Pregibon and P. S. Doyle, Optimization of encoded hydrogel particles for nucleic acid quantification, *Anal. Chem.*, 2009, **81**, 4873–4881.
30 C. L. Lewis, C. H. Choi, Y. Lin, C. S. Lee and H. Yi, Fabrication of uniform DNA-conjugated hydrogel microparticles via replica molding for facile nucleic acid hybridization assays, *Anal. Chem.*, 2010, **82**, 5851–5858.
31 R. D. Mitra and G. M. Church, In situ localized amplification and contact replication of many individual DNA molecules, *Nucleic Acids Res.*, 1999, **27**, e34.
32 C. Rieger, *et al.*, Polony analysis of gene expression in ES cells and blastocysts, *Nucleic Acids Res.*, 2007, **35**, e151.
33 S. Bigdeli, R. O. Dettloff, C. W. Frank, R. W. Davis and L. D. Crosby, A simple method for encapsulating single cells in alginate microspheres allows for direct PCR and whole genome amplification, *PLoS One*, 2015, **10**, e0117738.
34 S. Ma, *et al.*, Fabrication of microgel particles with complex shape via selective polymerization of aqueous two-phase systems, *Small*, 2012, **8**, 2356–2360.
35 M. Yanagisawa, S. Nigorikawa, T. Sakaue, K. Fujiwara and M. Tokita, Multiple patterns of polymer gels in microspheres due to the interplay among phase separation, wetting, and gelation, *Proc. Natl. Acad. Sci. U. S. A.*, 2014, **111**, 15894–15899.
36 T. Y. Lee, T. M. Choi, T. S. Shim, R. A. Frijns and S. H. Kim, Microfluidic production of multiple emulsions and functional microcapsules, *Lab Chip*, 2016, **16**, 3415–3440.
37 H. Domejean, *et al.*, Controlled production of sub-millimeter liquid core hydrogel capsules for parallelized 3D cell culture, *Lab Chip*, 2016, **17**, 110–119.
38 T. H. R. Niepa, *et al.* Microbial Nanoculture as an Artificial Microniche, *Sci. Rep.*, 2016, **6**, 30578.
39 J. Li, J. Lindley-Start, A. Porch and D. Barrow, Continuous and scalable polymer capsule processing for inertial fusion energy target shell fabrication using droplet microfluidics, *Sci. Rep.*, 2017, **7**, 6302.
40 S. Mytnyk, *et al.*, Microcapsules with a permeable hydrogel shell and an aqueous core continuously produced in a 3D microdevice by all-aqueous microfluidics, *RSC Adv.*, 2017, **7**, 11331–11337.
41 J. G. Werner, S. Nawar, A. A. Solovev and D. A. Weitz, Hydrogel Microcapsules with Dynamic pH-Responsive Properties from Methacrylic Anhydride, *Macromolecules*, 2018, **51**, 5798–5805.
42 T. Watanabe, I. Motohiro and T. Ono, Microfluidic Formation of Hydrogel Microcapsules with a Single Aqueous Core by Spontaneous Cross-Linking in Aqueous Two-Phase System Droplets, *Langmuir*, 2019, **35**, 2358–2367.
43 K. Vijayakumar, S. Gulati, A. J. de Mello and J. B. Edel, Rapid cell extraction in aqueous two-phase microdroplet systems, *Chem. Sci.*, 2010, **1**, 447–452.
44 N. D. Dinh, *et al.*, Functional reservoir microcapsules generated via microfluidic fabrication for long-term cardiovascular therapeutics, *Lab Chip*, 2020, **20**, 2756–2764.

45 B. D. Fairbanks, M. P. Schwartz, C. N. Bowman and K. S. Anseth, Photoinitiated polymerization of PEG-diacrylate with lithium phenyl-2,4,6-trimethylbenzoylphosphinate: polymerization rate and cytocompatibility, *Biomaterials*, 2009, **30**, 6702–6707.

46 G. M. Cruise, D. S. Scharp and J. A. Hubbell, Characterization of permeability and network structure of interfacially photopolymerized poly(ethylene glycol) diacrylate hydrogels, *Biomaterials*, 1998, **19**, 1287–1294.

47 G. Cebrian, S. Condon and P. Manas, Physiology of the Inactivation of Vegetative Bacteria by Thermal Treatments: Mode of Action, Influence of Environmental Factors and Inactivation Kinetics, *Foods*, 2017, **6**, 107.

48 J. Song, F. Babayekhorasani and P. T. Spicer, Soft Bacterial Cellulose Microcapsules with Adaptable Shapes, *Biomacromolecules*, 2019, **20**, 4437–4446.

49 L. S. Dorobantu, A. K. Yeung, J. M. Foght and M. R. Gray, Stabilization of oil-water emulsions by hydrophobic bacteria, *Appl. Environ. Microbiol.*, 2004, **70**, 6333–6336.

50 Z. W. Kang, A. Yeung, J. M. Foght and M. R. Gray, Hydrophobic bacteria at the hexadecane-water interface: Examination of micrometre-scale interfacial properties, *Colloids Surf., B*, 2008, **67**, 59–66.

51 J. M. S. Cabral, Cell partitioning in aqueous two-phase polymer systems, *Adv. Biochem. Eng./Biotechnol.*, 2007, **106**, 151–171.

52 G. M. Zijlstra, M. J. F. Michielsen, C. D. de Gooijer, L. A. van der Pol and J. Tramper, Hybridoma and CHO cell partitioning in aqueous two-phase systems, *Biotechnol. Prog.*, 1996, **12**, 363–370.

53 H. Walter and J. L. Anderson, Partition behavior of cells and soluble substances in two-polymer aqueous phase systems, Comments on Zaslavsky's general rule, *FEBS Lett.*, 1981, **131**, 73–76.

54 R. J. Meagher, *et al.*, End-labeled free-solution electrophoresis of DNA, *Electrophoresis*, 2005, **26**, 331–350.

55 R. A. Verlinden, D. J. Hill, M. A. Kenward, C. D. Williams and I. Radecka, Bacterial synthesis of biodegradable polyhydroxyalkanoates, *J. Appl. Microbiol.*, 2007, **102**, 1437–1449.

56 S. Chanprateep, Current trends in biodegradable polyhydroxyalkanoates, *J. Biosci. Bioeng.*, 2010, **110**, 621–632.

57 P. Spiekermann, B. H. A. Rehm, R. Kalscheuer, D. Baumeister and A. Steinbuchel, A sensitive, viable-colony staining method using Nile red for direct screening of bacteria that accumulate polyhydroxyalkanoic acids and other lipid storage compounds, *Arch. Microbiol.*, 1999, **171**, 73–80.

58 S. Hermawan and D. Jendrossek, Microscopical investigation of poly(3-hydroxybutyrate) granule formation in Azotobacter vinelandii, *FEMS Microbiol. Lett.*, 2007, **266**, 60–64.

59 J. Vaitekunas, R. Gasparaviciute, R. Rutkiene, D. Tauraite and R. Meskys, A 2-Hydroxypyridine Catabolism Pathway in Rhodococcus rhodochrous Strain PY11, *Appl. Environ. Microbiol.*, 2016, **82**, 1264–1273.